NANO · MICRO small
www.small-journal.com

Design Rules for Template-Confined DNA-Mediated Nanoparticle Assembly

*Wenjie Zhou, Qing-Yuan Lin, Jarad A. Mason, Vinayak P. Dravid, and Chad A. Mirkin**

Template-based strategies are becoming increasingly important for controlling the position of nanoparticle-based (NP-based) structures on surfaces for a wide variety of encoding and device fabrication strategies. Thus, there is an increasing need to understand the behavior of NPs in confined spaces. Herein, a systematic investigation of the diffusion and adsorption properties of DNA-modified NPs is presented in lithographically defined, high-aspect-ratio pores using a template-confined, DNA-mediated assembly. Leveraging the sequence-specific binding affinity of DNA, it is discovered that although NP adsorption in deep polymer pores follows a traditional Langmuir adsorption model when under thermodynamic control, such NPs kinetically follow Fick's classical law of diffusion. Importantly, these observations allow one to establish design rules for template-confined, DNA-mediated NP assembly on substrates based on pore dimensions, NP size and shape, NP concentration, temperature, and time. As a proof-of-concept example, these design rules are used to engineer a vertical, four-layer assembly consisting of individual octahedral NPs stacked on top of one another, with in-plane positioning defined by pores generated by e-beam lithography.

1. Introduction

Nanoparticles (NPs), due to their small size, well-defined shapes,[1–4] and unusual properties,[5–16] are promising ideal building blocks for constructing higher-ordered materials.[10,17–19] DNA, due to its sequence programmability and adjustable length, has become a versatile tool for making highly ordered materials from NP building blocks,[20–22] both in solution and on surfaces.[17,19,20,22–29] Indeed, we and others have used programmable assembly to map out the design space for NP superlattices of over 500 different crystal types spanning over 40 different lattice symmetries and 4 different crystal habits.[20–22,24–27] Moreover, we recently showed that a wide variety of structures not attainable through conventional top-down lithographic methods could be made using a combination of top-down lithographic and bottom-up DNA-programmable assembly,[17,19,29] thereby establishing a platform for the metamaterial community to consider a more diverse set of architectures to discover, design, and realize unusual NP-based materials with desirable properties.

The design and synthesis of these new colloidal NP surface architectures will benefit from an improved understanding of the fundamental diffusion and adsorption behaviors of NPs on surfaces and in confined environments. Although the behavior of solution-dispersed NPs has been extensively studied using well-established theoretical[30] and analytical techniques,[31–33] there are comparatively few studies[34,35] of NP interactions with surfaces due to the complexity of interactions involved and a lack of reasonable experimental models. Recently, we found that despite the complex interactions between NPs and surfaces, NP adsorption on flat surfaces can be described by a simple Langmuir adsorption isotherm,[36] which is normally used to model molecular surface adsorption. This work established an initial understanding of the collective interactions between ligand-functionalized NPs and a flat surface with complementary binding sites. In less ideal situations, flat-surface-bound binding sites cannot be guaranteed, and a substantial number of NP-surface interactions involve degrees of physical confinement on the NP. For instance, in directed NP assembly systems,[17–19,29] NP adsorption – and the quality of the final structure – is not only dependent on the NP interactions with lithographically defined pores, but also with the surface at the base of the pores. Such interactions are challenging, if not impossible, to directly observe in situ with existing characterization techniques. Therefore, in order to understand the diffusion and adsorption of NPs in porous environments, a suitable model or platform to investigate such behavior is required.

The behavior of NPs is strongly governed by Brownian motion; hence tracking individual NP interactions with a surface covered by a porous template is experimentally challenging. Given the difficulty of studying such interactions in situ, we adopted a recently developed template-confined, DNA-mediated assembly technique to investigate NP adsorption thermodynamics and kinetics.[19] This technique involves using electron beam lithography (EBL) to fabricate 1D pore channels at fixed

W. Zhou, Dr. J. A. Mason, Prof. C. A. Mirkin
Department of Chemistry and International Institute for Nanotechnology
Northwestern University
2145 Sheridan Road, Evanston, IL 60208, USA
E-mail: chadnano@northwestern.edu
Dr. Q.-Y. Lin, Prof. V. P. Dravid, Prof. C. A. Mirkin
Department of Materials Science and Engineering
Northwestern University
2220 Campus Drive, Evanston, IL 60208, USA
The ORCID identification number(s) for the author(s) of this article can be found under https://doi.org/10.1002/smll.201802742.

DOI: 10.1002/smll.201802742

positions in a poly(methyl methacrylate) (PMMA) polymer thin film on a gold-coated silicon substrate with a specific DNA sequence covalently attached to the exposed gold at the base of each pore. This approach offers a highly programmable system where critical diffusive and adsorptive parameters such as pore diameter, pore depth, NP shape, NP concentration, temperature, and time can be precisely and independently defined.

Herein, a statistical approach was designed and utilized to analyze and describe NP diffusion and adsorption in porous templates. Briefly, we investigate the relationships between adsorption yield and NP size, NP concentration, pore size, pore depth, temperature, and time. The diffusion and adsorption behaviors of NPs were studied under both equilibrium and nonequilibrium conditions. From this analysis, we show how pore diameter and depth are directly related to particle adsorption yield as well as the time required to reach equilibrium. Remarkably, despite the complexity of the system and the large size of the NP building blocks (compared with the size of molecules), particle diffusion and adsorption in this system are well described and modeled using Fick's diffusion law and the Langmuir adsorption model, thereby making it possible to predict both the kinetic and thermodynamic behavior of NPs in pores.

2. Results and Discussion

In a typical experiment, 1D pore channels were designed and fabricated using EBL to pattern nanoscale circular pores ranging from 40 to 220 nm in diameter and 100 to 600 nm in depth in PMMA thin films deposited on gold-coated silicon substrates (**Figure 1**).[17,19] Subsequently, DNA-mediated NP assembly (diffusion and adsorption) within these pores was studied over a temperature range of 25 to 45°C and time periods of 0.5 to 96 h. After assembly of the DNA-modified NPs, the PMMA template was removed to allow the NP arrays to be transferred intact from the solution phase to the solid state. The adsorption yield, θ, where $\theta = \frac{N_{\text{occupied}}}{N_{\text{total}}}$ (N_{occupied} is the number of NP-occupied binding sites, while N_{total} is the total number of potential binding sites), was calculated based upon NP position data taken from scanning electron microscopy (SEM) measurements (Figure 1).

In this system, pore size plays a key role in controlling the degree of physical confinement. Qualitatively, NPs cannot diffuse into pores whose diameters are too narrow, while pores that are too wide tend to be filled with multiple NPs. However, a quantitative relationship between pore size and the adsorption yield at the single particle level remains unknown. To systematically address this problem, we performed a series of experiments under equilibrium conditions, where only the pore size was varied. To ensure the system was in an equilibrium state, each experimental condition was carried out for multiple lengths of time, and the adsorption yields were calculated. When an increase in time no longer led to a measurable increase in yield, the system was deemed to have reached

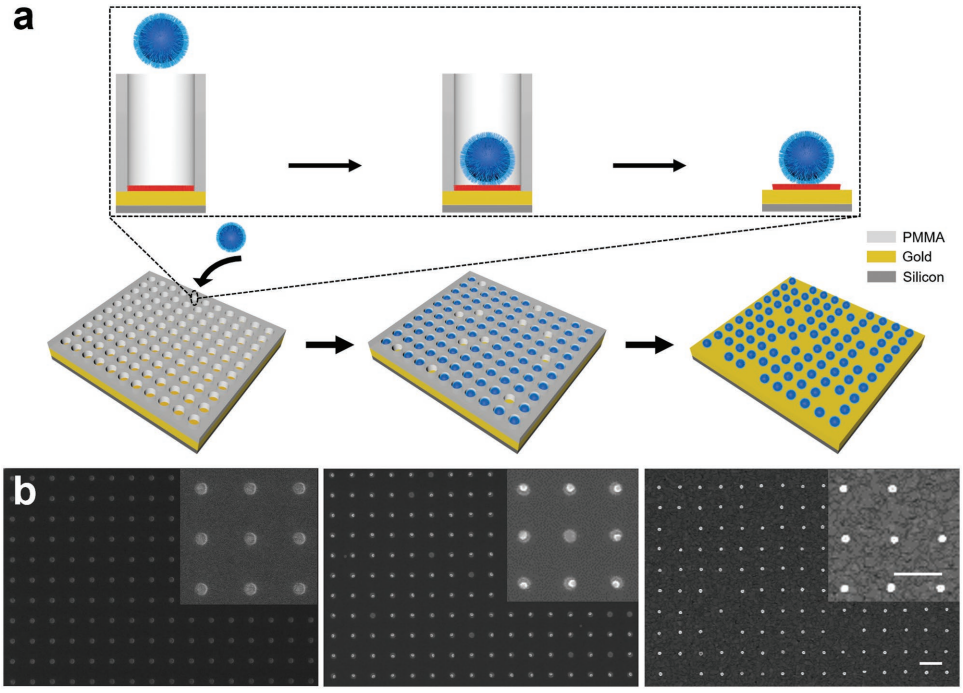

Figure 1. Scheme and SEM characterization of template-confined, DNA-mediated NP assembly. a) Arrays of nanoscale pores are fabricated using EBL, after which both NPs and the bottom of each pore are densely functionalized with thiolated DNA (red and blue indicates complementary DNA sequences). By designing the NPs to have a terminal DNA sequence complementary to that at the bottom of pores, NPs are adsorbed onto surfaces at precisely defined locations. The porous polymer templates are removed to generate solid-state NP arrays after assembly. b) SEM images of polymer templates (left), NPs assembled in the templates (middle), and NP arrays with the templates removed (right). Note that three images were captured from three separated samples prepared with the same experimental conditions. Scale bars, 500 nm.

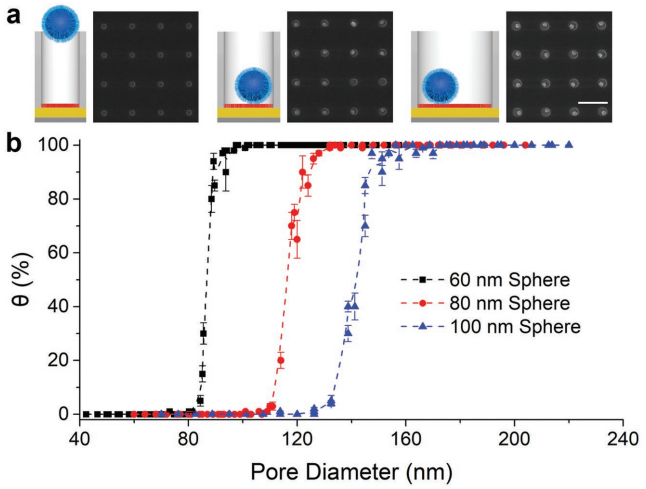

Figure 2. Effect of pore diameter on assembly yield. a) Scheme and SEM images of 80 nm diameter spherical NPs assembled into nanopores with different sizes (pore diameters = 100, 130, and 200 nm, from left to right) under equilibrium conditions. Scale bar, 500 nm. b) Assembly yield as a function of pore diameter in which 60, 80, and 100 nm diameter spherical NPs were assembled at equilibrium. All pore depths are 200 nm, assembly temperature is 25 °C, NP concentrations are 150 pM, and assembly times are longer than 48 h. Each data point represents an average of two independent experiments, 900 sites were counted for each experiment, with an error bar as the standard deviation.

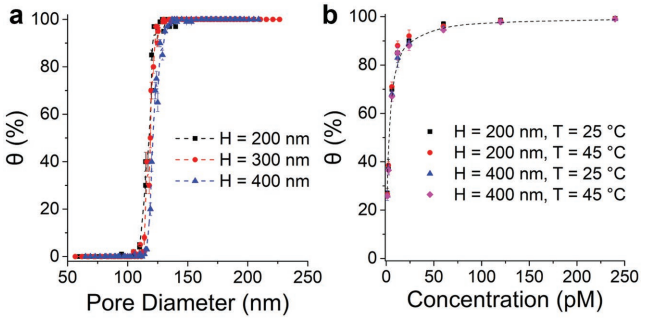

Figure 3. Thermodynamic analysis of NP assembly in pores. a) Assembly yield as a function of pore size. Spherical NPs (diameter = 80 nm, concentration = 150 pM) were adsorbed in nanopores (depth = 200, 300, and 400 nm) at a temperature of 25 °C for at least 96 h. b) Assembly yield as a function of NP concentration. Spherical NPs (diameter = 80 nm) were adsorbed in nanopores (diameter = 140 nm, depth = 200 and 400 nm) at a temperature of 25 and 45 °C for at least 96 h. Each data point represents an average of two independent experiments, 900 sites were counted for each experiment, with an error bar as the standard deviation.

equilibrium. Adsorption yield is plotted as a function of pore size for various sizes of NPs and exhibits a sigmoidal shape with a sharp transition (**Figure 2**). It should be noted that the DNA sequences[17,19] (DNA sequences are specified in Table S2 in the Supporting Information) used in this experiment add ≈20 nm to the diameter of the gold core for each NP. Interestingly, the minimum pore diameter required to achieve 100% adsorption yield is consistently ≈1.4 times the diameter of the DNA-functionalized spherical NP. This is a general guideline to maximize adsorption yield while maintaining positional control. In addition, the transition from 0% to 100% yield occurs across a consistent pore size to NP diameter (hydrodynamic diameter, which includes the ligand shell) ratio of 1.1–1.4 when the pore depth is at least 200 nm. Importantly, this indicates that in order for NPs to diffuse through polymer nanopores, a pore size of at least 1.1 times the total size of a NP (including ligand shell) is required. However, to reach 100% occupancy, pore sizes of at least 1.4 times the NP size are necessary.

In addition to pore diameter, pore depth also affects the physical confinement of the NPs, with deeper pores expected to provide stronger confinement. However, it is unknown whether pore depth affects the thermodynamics of NP adsorption. It was previously shown that DNA-mediated NP adsorption on flat surface follows the Langmuir adsorption model in the equilibrium state,[36] but it is unclear if the same model applies under strong physical confinement in pores. In the Langmuir adsorption model, the relationship of surface coverage and adsorption parameters is described as $c(1-\theta)\,k_a = \theta k_d$, where c is the concentration of NPs; k_a and k_d are the adsorption and desorption rate constants, respectively. By further defining $K_L = \frac{k_a}{k_d}$, the equation can be simplified to $\theta = \frac{K_L c}{1+K_L c}$. If the NP concentration in solution is held constant, k_a should describe both adsorption to the DNA-mediated binding sites and diffusion through the pore, because adsorption events occur at the bottom of pores. Likewise, desorption processes combine both desorption from binding sites and diffusion out of the pore. It is unclear whether changing the diffusion length will affect k_a, or k_b, and thus K_L, as well as the relationship between pore size and adsorption yield.

To elucidate the effect of pore depth on the thermodynamics of NP adsorption, we carried out experiments with pores of various depths (H = 100, 200, 300, 400 nm) and diameters (110 and 140 nm, Figure S3, Supporting Information). For 80 nm diameter NPs, we found consistent adsorption yields for both small (110 nm) and large diameter pores (140 nm), regardless of pore depth. These experiments show that, for the conditions explored here, θ is independent of pore depth (**Figure 3**a). This result indicates that under equilibrium conditions, pore depth does not alter the thermodynamics of NP adsorption. To further test whether K_L varies with pore depth, we investigated θ as a function of NP concentration. The results show that NP adsorption in high-aspect-ratio pores still fits the Langmuir adsorption model (Figure 3b). In fact, K_L values for different pore depths at temperatures below the DNA melting temperature are nearly constant. This further indicates that pore depth does not influence the equilibrium result of NP surface adsorption. Given sufficient time to reach equilibrium, NPs diffuse through deep pores with high aspect ratios, indicating that deep pores can be used to provide a high degree of physical confinement without compromising adsorption yield.

While pore depth does not affect the thermodynamics of NP adsorption, it does significantly affect the kinetics of NP adsorption, where deeper pores increase the time required to reach equilibrium. To quantify how the kinetics of NP diffusion are affected, we designed a series of ex situ experiments to investigate the relationship between θ and assembly time for pore depths of 100, 200, 300, 400, and 600 nm (**Figure 4**a).

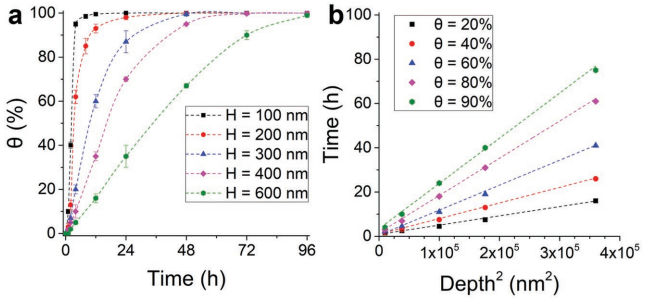

Figure 4. Kinetic analysis of NP diffusion in pores. a) Assembly yield as a function of assembly time. Spherical NPs (diameter = 80 nm, concentration = 150 pM) were adsorbed in nanopores (diameter = 140 nm, depth = 100, 200, 300, 400, and 600 nm) at 25 °C for varying time periods. Each data point represents an average of two independent experiments, with an error bar as the standard deviation. b) The time required to reach 20%, 40%, 60%, 80%, and 90% yields is plotted as a function of the square of pore depth.

Importantly, we found that the diffusion of NPs during adsorption in nanopores can be rationalized using Fick's laws of diffusion, which describe the diffusion flux of molecules from high-concentration (high chemical potential) to low-concentration regions (low chemical potential). In our template-confined DNA-mediated assembly system, each pore effectively represents a 1D channel for NP diffusion. As soon as the nanopores are immersed in a colloidal NP solution, the NPs begin to diffuse from a high-concentration region (solution) to a low – effectively zero – concentration region (the bottom of each pore). It should be noted that the interactions between the DNA shell and PMMA walls are assumed to be collision only. Such an assumption is applicable in DNA-mediated surface assembly, where DNA:NP size ratios are designed to be small in order to maintain the shape of NPs. Using a simplified 1D diffusion model, the NP concentration at the bottom of each pore can be calculated using Fick's law:[37]

$$c(H,t) = c_o \,\mathrm{erfc}\left(\frac{H}{2\sqrt{Dt}}\right) \quad (1)$$

where c represents the diffusive concentration at a distance H from the environment (top of pore) after a dissolution time, t, c_o is the environmental concentration, D is the diffusion coefficient, and erfc is the complementary error function. As previously discussed, template-confined, DNA-mediated assembly satisfies the Langmuir adsorption model, which indicates that the same surface coverage is determined by the NP concentration, strength of interaction between the NP and surface, ratio of pore diameter to NP size, and temperature, but not by the pore depth. As a result, the adsorption yield for various pore depths, $\frac{H}{2\sqrt{Dt}}$ must be constant ($H > 0$, $\theta \leq 1$), indicating that the assembly time must be directly proportional to the square of the pore depth (i.e., $t \propto H^2$). We calculated the assembly time required to reach 20%, 40%, 60%, 80%, and 90% yield for pores of 100, 200, 300, 400, and 600 nm in depth, respectively (Figure 4a). As predicted by Fick's law, the results show that the assembly time is indeed proportional to the square of pore depth, (Figure 4b). This confirmed that, despite the complexity of the system, classical molecular diffusion models can be utilized to describe the diffusive behavior of NPs, improving our fundamental understanding of NP behaviors in confined environments.[17,19,38]

While we focused on spherical NPs, the adsorption behavior can be extended to anisotropic NPs. Specifically, we found that the effective diameters of sphere-like anisotropic NPs (as compared with their spherical counterparts) are described by the diameter of the smallest sphere required to circumscribe the anisotropic NP. For cubic NPs, the effective diameter is $\sqrt{3}$ times the cube edge length; while, for octahedral NPs, the effective diameter is $\sqrt{2}$ times the edge length. Equilibrium adsorption yields were plotted as functions of pore sizes for spherical NPs with diameters of 80 nm, cubic NPs with edge lengths of 80 nm, and octahedral NPs with edge lengths of 80 nm (**Figure 5**). Cubes of this size should effectively behave as a sphere with a diameter of 140 nm, and therefore the minimal pore size required for 100% yield should be 215 nm (including a 20 nm DNA shell); for octahedra, the corresponding pore size should be 180 nm. The experimental results agree closely with the expected pore size (Figure 5). Such behavior is primarily under the control of rapid Brownian motion; the anisotropy of NPs plays a negligible role in the interaction between NPs and pores.

As a proof-of-concept, we show how the fundamental relationships elucidated in this work can be leveraged to synthesize sophisticated nanostructures with a high degree of structural control. Specifically, we targeted the assembly of four-layer NP architectures, (**Figure 6**). Gold octahedra with an average edge length of 80 nm were synthesized and functionalized with DNA. To direct NP assembly, PMMA nanopores (180 nm diameter, 400 nm depth) were patterned on a gold-coated Si substrate. DNA-mediated layer-by-layer assembly was then used to grow the 1st (60 h), 2nd (48 h), 3rd (24 h), and 4th (12 h)

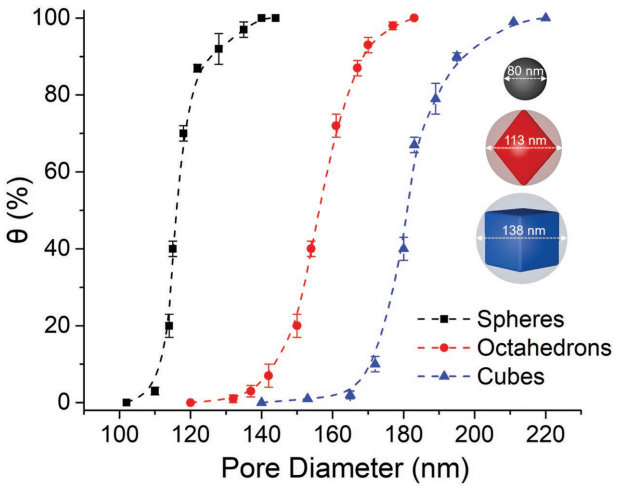

Figure 5. Effect of NP shape on assembly yield. Assembly yield as a function of pore diameter with different shapes of NPs assembled at equilibrium. Assembled NPs are spherical NPs with 80 nm in diameter, octahedron NPs with 80 nm in edge length, cubic NPs with 80 nm in edge length. The effective sizes of anisotropic NPs are essentially the diameter of their circumscribed spheres, which is the effective shape under strong Brownian motion in solution. All pore depths are 200 nm, assembly temperature is 25 °C, assembly times are longer than 48 h. Each data point represents an average of three independent experiments, 400 sites were counted for each experiment, with the error bar as the standard deviation.

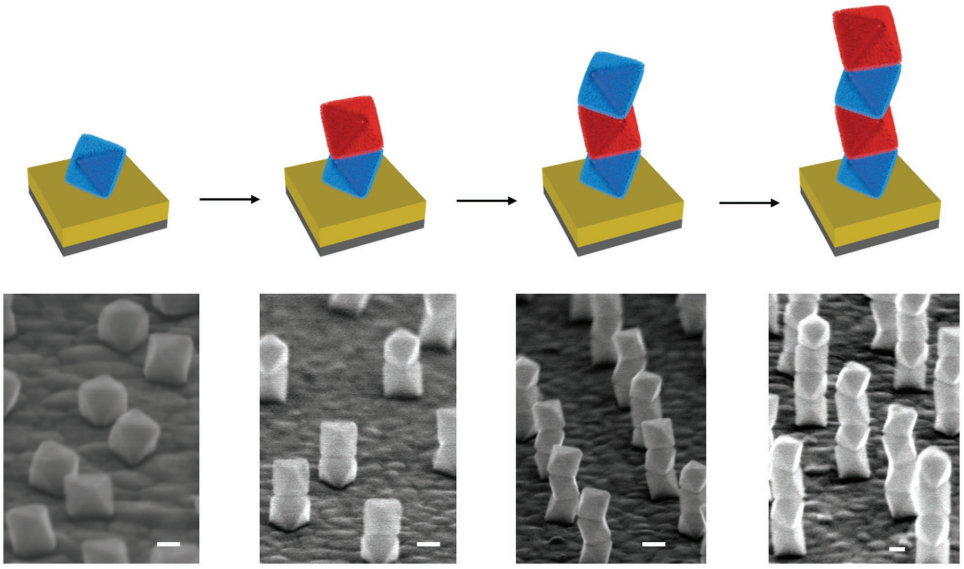

Figure 6. Template-confined vertical assembly of one-, two-, three-, and four-layer architectures of octahedral NPs. Guided by PMMA nanopores (diameter = 165 nm, depth = 400 nm), octahedral NPs (edge length = 80 nm) are assembled layer-by-layer through DNA-mediated assembly. NP architectures show good facet registry, which leads to high stability of assembled structures. Different colors represent octahedral NPs capped with different DNA sequences, where blue is complementary to red (sequence details are listed in Supporting Information). Scale bars: 50 nm, tilting angle of SEM images: 70°.

layers in successive fashion. Less time was required for each successive layer since the pore depth decreases with the addition of each layer. SEM characterization confirmed that the NPs assembled in high yield (>90%), with near perfect facet registry among the two-, three-, and four-layer structures. As compared with the previous three-layer structures assembled using this technique,[19] the assembly yield is significantly higher than the reported results (≈70%). Therefore, this fundamental study of NP adsorption thermodynamics and kinetics allows one to significantly improve the yield of multilayer NP architectures and should allow researchers to program and realize even more sophisticated structures in the future.

3. Conclusion

In conclusion, this work provides valuable insight into the thermodynamic and kinetic considerations of colloidal NP assembly, which can be generalized for other systems where the interactions between NPs and pores play a crucial role.[39–46] The design rules elucidated by this work:

Rule 1: Minimal NP concentration for a desired adsorption yield can be predicted for specific NPs, since the relationship between adsorption yield in pores and NP concentration at equilibrium can be described by the Langmuir adsorption equation, where $\theta = \frac{K_L c}{1 + K_L c}$.

Rule 2: Minimal required assembly time can be predicted for pores of specific depths, since the relationship between assembly time and pore depth at fixed adsorption yield follows Fick's law, where $t \propto H^2$.

Rule 3: To maximize NP adsorption, the pore radius should be ≥1.4 times the hydrodynamic radius of the adsorbing NPs.

Rule 4: For pseudo-spherical anisotropic NPs (e.g., cubes and octahedra), the size can be approximated based upon the diameter of the smallest sphere required to circumscribe such NPs.

Rule 5: Equilibrium adsorption yield is independent of pore depth.

will significantly advance the level of structural control that is possible when using NPs as building blocks for generating structurally and compositionally sophisticated and complex particle-based architectures.[19] With the diversity of NP shapes, sizes, and compositions that can serve as building blocks,[47] the lessons learned from this work will be extremely valuable for the design, synthesis, and integration of NP-based materials relevant to applications in biology,[39,43] optics,[17,19] and catalysis.[44,45]

4. Experimental Section

Spherical gold NPs capped with citrate ligands with nominal diameters of 60, 80, and 100 nm were purchased from Ted Pella, Inc. and used as received. Single crystalline gold nanocubes and octahedrons were synthesized via the seed-mediated method described in detail by O'Brien et al.[4] Briefly, uniform, single crystalline spherical gold NPs were synthesized via an iterative chemical refinement process. These NPs were subsequently used as "seeds" to template the growth of cubes. Importantly, this synthetic procedure results in structurally uniform anisotropic NPs produced with high yield.

PMMA pores were fabricated on Au-coated Si substrates with EBL. First, a Si wafer was cleaned via an O_2 plasma (≈0.2 mbar) at 50 W for 5 min. Following plasma cleaning, a 5 nm Cr adhesion layer, followed by a 100 nm Au layer were deposited onto the Si substrate with electron beam evaporation, at a rate of 0.25 Å s^{-1} (Kurt J. Lesker Company). The wafer was then cut into smaller pieces (1.5 × 1.5 cm^2) and stored in vacuum desiccator. Substrates were then spin-coated with positive e-beam resist PMMA. The thickness and spin-coating parameters are specified in Table S1 in the Supporting Information. The PMMA was baked at

200 °C for 60 s, followed by EBL (FEI Quanta 650 ESEM) to define the size and position of the pores. An accelerating voltage of 30 kV with a dosage of 200–1500 μC cm^{-2} was used to pattern pores with 90–260 nm diameters. The substrates were developed in a methyl isobutyl ketone/isopropyl alcohol (IPA) 1:3 solution for 60 s, rinsed with IPA, and blown dry with N_2. After development, each substrate was cleaned via O_2 plasma (≈0.2 mbar) at 50 W for 1 min to remove potential PMMA residue at the bottom of pores and cut into four smaller pieces to fit in 2 mL Eppendorf tubes.

The DNA sequences used in this work are given in Table S2 in the Supporting Information. In brief, we functionalized substrates and NPs with orthogonal 3′ thiolated DNA sequences, denoted as X and Y, respectively. Then, complementary linker DNA strands were hybridized to both the NPs and the substrate to provide rigidity to the DNA shell. Each linker strand possessed a short 5-base terminus designed to link the NPs to the substrates through complementary DNA hybridization events.

NPs were functionalized as described by Jones et al.[25] and O'Brien et al.[36] In brief, 3′ alkylthiol-modified oligonucleotides were first treated with a 100 × 10^{-3} M solution of dithiothreitol (DTT) in 170 × 10^{-3} M sodium phosphate buffer (pH = 7.4), followed by purification on a Nap-5 size exclusion column (GE Life Sciences) to remove DTT. During this time, 1 mL aliquots of the cube solutions were centrifuged for 8 min at 6000–10 000 rpm depending on the shapes of the NPs, the supernatant was removed, and the NPs were resuspended in water. The NPs were then centrifuged a second time, the supernatant was removed, and then the purified DNA and water were immediately added to the pellet. Specifically, 5 μmol of thiolated DNA was added per 1 mL of original NP solution. The NP solution was then brought to 0.01 M sodium phosphate buffer (pH = 7.4) and 0.01 wt% sodium dodecyl sulfate (SDS) in water. Stepwise addition of 2 M NaCl was carried out every half hour, such that the NaCl concentration was stepped through 0.05, 0.1, 0.2, 0.3, 0.4 M, and finally arrived at 0.5 M. Following this process, the NPs were placed on a shaker at 1000 rpm and left overnight to ensure a dense loading of oligonucleotides. After functionalization, the NP solutions were centrifuged three times to remove excess DNA. After each of the first two rounds of centrifugation, NPs were resuspended in 0.01 wt% SDS, and after the last centrifugation step, the NPs were resuspended in 0.5 M NaCl, 0.01 M sodium phosphate buffer (pH = 7.4), and 0.01 wt% SDS solution.

For the functionalization of the substrate with DNA, the procedure was similar as described above. Specifically, 1 μmol of DTT-cleaved DNA in water was added to each substrate. However, instead of stepwise addition of NaCl, the substrates were brought to 1 M NaCl in one addition, and then shaken for 1 h at 1000 rpm. Substrates were then rinsed three times with water and placed in a 0.5 M NaCl, 0.01 M sodium phosphate buffer (pH = 7.4), and 0.01 wt% SDS solution.

After functionalization of thiolated DNA strands, linker strands were hybridized to both the substrates and NPs. To determine the appropriate number of linkers, the concentration of the NP solution was measured using UV–vis.[48] Subsequently, 10 000 strands of linkers were added per NP. Substrates were incubated in a solution containing 0.5 × 10^{-6} M linker. Both the substrates and the NP solutions were then heated to 55 °C for 30 min, and then allowed to slowly cool to room temperature to ensure full hybridization between anchor and linker DNA sequences.

Following linker hybridization, the substrates were rinsed in 0.5 M NaCl, 0.01 M sodium phosphate buffer, and 0.01 wt% SDS solution three times, while NPs were used without further processing. For the assembly of NPs, substrates were first placed in the NP solution and shaken at 1000 rpm for varying time (0.5–96 h) and at variant temperature (25 to 45 °C). After assembly, the substrates were rigorously rinsed three times in 0.5 M NaCl, 0.01 M sodium phosphate buffer, and 0.01 wt% SDS solutions to remove unbounded NPs. Then the substrates were immersed in 80% IPA in water (by volume) with 0.2 M ammonium acetate (AA) at 45 °C for 30 min to fully remove the PMMA. After PMMA removal, the substrates were rinsed three times with a solution of 80% IPA and 0.2 M AA, then blown dried with N_2.

Supporting Information

Supporting Information is available from the Wiley Online Library or from the author.

Acknowledgements

This material is based upon work supported by the Air Force Office of Scientific Research Awards FA9550-12-1-0280, FA9550-14-1-0274, and FA9550-17-1-0348. This work made use of the EPIC facility of the NU*ANCE* Center at Northwestern University, which has received support from the Soft and Hybrid Nanotechnology Experimental (SHyNE) Resource (NSF NNCI-1542205); the MRSEC program (NSF DMR-1720139) at the Materials Research Center; the Keck Foundation, and the State of Illinois, through the IIN.

Conflict of Interest

The authors declare no conflict of interest.

Keywords

adsorption, DNA-mediated assembly, gold nanoparticles, kinetics, thermodynamics

Received: July 13, 2018
Revised: August 17, 2018
Published online:

[1] R. C. Jin, Y. W. Cao, C. A. Mirkin, K. L. Kelly, G. C. Schatz, J. G. Zheng, *Science* **2001**, *294*, 1901.
[2] M. Liu, P. Guyot-Sionnest, *J. Phys. Chem. B* **2005**, *109*, 22192.
[3] S. Eustis, M. A. El-Sayed, *J. Appl. Phys.* **2006**, *100*, 044324.
[4] M. N. O'Brien, M. R. Jones, K. A. Brown, C. A. Mirkin, *J. Am. Chem. Soc.* **2014**, *136*, 7603.
[5] C. L. Nehl, H. Liao, J. H. Hafner, *Nano Lett.* **2006**, *6*, 683.
[6] K. L. Kelly, E. Coronado, L. L. Zhao, G. C. Schatz, *J. Phys. Chem. B* **2003**, *107*, 668.
[7] R. Narayanan, M. A. El-Sayed, *Nano Lett.* **2004**, *4*, 1343.
[8] N. Yan, J. Zhang, Y. Yuan, G.-T. Chen, P. J. Dyson, Z.-C. Li, Y. Kou, *Chem. Commun.* **2010**, *46*, 1631.
[9] R. Narayanan, M. A. El-Sayed, *J. Phys. Chem. B* **2005**, *109*, 12663.
[10] J. I. Cutler, E. Auyeung, C. A. Mirkin, *J. Am. Chem. Soc.* **2012**, *134*, 1376.
[11] C. M. Calabrese, T. J. Merkel, W. E. Briley, P. S. Randeria, S. P. Narayan, J. L. Rouge, D. A. Walker, A. W. Scott, C. A. Mirkin, *Angew. Chem., Int. Ed.* **2015**, *54*, 476.
[12] C. Zhang, L. L. Hao, C. M. Calabrese, Y. Zhou, C. H. J. Choi, H. Xing, C. A. Mirkin, *Small* **2015**, *11*, 5360.
[13] A. F. Radovic-Moreno, N. Chernyak, C. C. Mader, S. Nallagatla, R. S. Kang, L. L. Hao, D. A. Walker, T. L. Halo, T. J. Merkel, C. H. Rische, S. Anantatmula, M. Burkhart, C. A. Mirkin, S. M. Gryaznov, *Proc. Natl. Acad. Sci.* **2015**, *112*, 3892.
[14] G. Goya, T. Berquo, F. Fonseca; M. Morales, *J. Appl. Phys.* **2003**, *94*, 3520.
[15] W. S. Seo, H. H. Jo, K. Lee, B. Kim, S. J. Oh, J. T. Park, *Angew. Chem., Int. Ed.* **2004**, *43*, 1115.
[16] T.-J. Park, G. C. Papaefthymiou, A. J. Viescas, A. R. Moodenbaugh, S. S. Wong, *Nano Lett.* **2007**, *7*, 766.

[17] Q. Y. Lin, Z. Y. Li, K. A. Brown, M. N. O'Brien, M. B. Ross, Y. Z. S. Butun, S. Butun, P. C. Chen, G. C. Schatz, V. P. Dravid, K. Aydin, C. A. Mirkin, *Nano Lett.* **2015**, *15*, 4699.
[18] V. Flauraud, M. Mastrangeli, G. D. Bernasconi, J. Butet, D. T. Alexander, E. Shahrabi, O. J. Martin, J. Brugger, *Nat. Nanotechnol.* **2017**, *12*, 73.
[19] Q.-Y. Lin, J. A. Mason, Z. Li, W. Zhou, M. N. O'Brien, K. A. Brown, M. R. Jones, S. Butun, B. Lee, V. P. Dravid, K. Aydin, C. A. Mirkin, *Science* **2018**, *359*, 669.
[20] R. J. Macfarlane, B. Lee, M. R. Jones, N. Harris, G. C. Schatz, C. A. Mirkin, *Science* **2011**, *334*, 204.
[21] R. J. Macfarlane, M. R. Jones, B. Lee, E. Auyeung, C. A. Mirkin, *Science* **2013**, *341*, 1222.
[22] C. A. Mirkin, R. L. Letsinger, R. C. Mucic, J. J. Storhoff, *Nature* **1996**, *382*, 607.
[23] M. Oh, C. A. Mirkin, *Nature* **2005**, *438*, 651.
[24] S. Y. Park, A. K. R. Lytton-Jean, B. Lee, S. Weigand, G. C. Schatz, C. A. Mirkin, *Nature* **2008**, *451*, 553.
[25] M. R. Jones, N. C. Seeman, C. A. Mirkin, *Science* **2015**, *347*, 1260901.
[26] Y. Kim, R. J. Macfarlane, M. R. Jones, C. A. Mirkin, *Science* **2016**, *351*, 579.
[27] E. Auyeung, T. Li, A. J. Senesi, A. L. Schmucker, B. C. Pals, M. O. de la Cruz, C. A. Mirkin, *Nature* **2014**, *505*, 73.
[28] D. Nykypanchuk, M. M. Maye, D. Van Der Lelie, O. Gang, *Nature* **2008**, *451*, 549.
[29] Q.-Y. Lin, E. Palacios, W. Zhou, Z. Li, J. A. Mason, Z. Liu, H. Lin, P.-C. Chen, V. P. Dravid, K. Aydin, *Nano Lett.* **2018**, *18*, 2645.
[30] P. F. Damasceno, M. Engel, S. C. Glotzer, *Science* **2012**, *337*, 453.
[31] E. Navarro, A. Baun, R. Behra, N. B. Hartmann, J. Filser, A.-J. Miao, A. Quigg, P. H. Santschi, L. Sigg, *Ecotoxicology* **2008**, *17*, 372.
[32] A. S. Stender, N. Fang, *MRS Online Proc. Library Archive* **2013**, *1546*.
[33] N. K. Maurya, A. Mandal, *Pet. Sci. Technol.* **2016**, *34*, 429.
[34] L. Malaquin, T. Kraus, H. Schmid, E. Delamarche, H. Wolf, *Langmuir* **2007**, *23*, 11513.
[35] K. Mertens, V. Putkaradze, D. Xia, S. Brueck, *J. Appl. Phys.* **2005**, *98*, 034309.
[36] M. N. O'Brien, B. Radha, K. A. Brown, M. R. Jones, C. A. Mirkin, *Angew. Chem., Int. Ed.* **2014**, *53*, 9532.
[37] A. Fick, *J. Membr. Sci.* **1995**, *100*, 33.
[38] C. Kuemin, L. Nowack, L. Bozano, N. D. Spencer, H. Wolf, *Adv. Funct. Mater.* **2012**, *22*, 702.
[39] A. Ragusa, I. GarcÍa, S. PenadÉs, *IEEE Trans. NanoBiosci.* **2007**, *6*, 319.
[40] D. Cai, J. M. Mataraza, Z.-H. Qin, Z. Huang, J. Huang, T. C. Chiles, D. Carnahan, K. Kempa, Z. Ren, *Nat. Methods* **2005**, *2*, 449.
[41] X. Hu, S. Dong, *J. Mater. Chem.* **2008**, *18*, 1279.
[42] G. G. Wildgoose, C. E. Banks, R. G. Compton, *Small* **2006**, *2*, 182.
[43] A. J. Haes, R. P. Van Duyne, *J. Am. Chem. Soc.* **2002**, *124*, 10596.
[44] D. Astruc, F. Lu, J. R. Aranzaes, *Angew. Chem., Int. Ed.* **2005**, *44*, 7852.
[45] M. Haruta, *Chem. Rec.* **2003**, *3*, 75.
[46] G. J. Hutchings, *Chem. Commun.* **2008**, 1148.
[47] C. Zhang, R. J. Macfarlane, K. L. Young, C. H. J. Choi, L. L. Hao, E. Auyeung, G. L. Liu, X. Z. Zhou, C. A. Mirkin, *Nat. Mater.* **2013**, *12*, 741.
[48] M. N. O'Brien, M. R. Jones, K. A. Brown, C. A. Mirkin, *J. Am. Chem. Soc.* **2014**, *136*, 7603.